doi:10.1093/jmcb/mjy045
Published online August 22, 2018

Article

IFN-stimulated $P2Y_{13}$ protects mice from viral infection by suppressing the cAMP/EPAC1 signaling pathway

Chengfei Zhang†, Yan Yan†, Hongwang He, Li Wang, Na Zhang, Jie Zhang, Hongjun Huang, Nannan Wu, Hua Ren, Min Qian, Mingyao Liu, and Bing Du*

Shanghai Key Laboratory of Regulatory Biology, Institute of Biomedical Sciences and School of Life Sciences, East China Normal University, Shanghai 200241, China

† These authors contributed equally to this work.

* Correspondence to: Bing Du, E-mail: bdu@bio.ecnu.edu.cn

Edited by Bing Su

Among the most important sensors of extracellular danger signals, purinergic receptors have been demonstrated to play crucial roles in host defense against infection. However, the function of P2 receptors in viral infection has been little explored. Here we demonstrated that $P2Y_{13}$ and its ligand ADP play an important role in protecting hosts from viral infections. First, we demonstrate that $P2Y_{13}$, as a typical interferon-stimulated gene, is induced together with extracellular ADP during viral infection. Most importantly, extracellular ADP restricts the replication of different kinds of viruses, including vesicular stomatitis virus, Newcastle disease virus, herpes simplex virus 1, and murine leukemia virus. This kind of protection is dependent on $P2Y_{13}$ but not $P2Y_1$ or $P2Y_{12}$, which are also considered as receptors for ADP. Furthermore, cyclic adenosine monophosphate and EPAC1 are downregulated by extracellular ADP through the $P2Y_{13}$-coupled Gi alpha subunit. Accordingly, inhibition or deletion of EPAC1 significantly eliminates ADP/$P2Y_{13}$-mediated antiviral activities. Taken together, our results show that $P2Y_{13}$ and ADP play pivotal roles in the clearance of invaded virus and have the potential as antiviral targets.

Keywords: ADP, $P2Y_{13}$, ISG, cAMP, viral infection

Introduction

Upon viral infection, the host can sense the virus through the recognition of pathogen-associated molecular patterns by pattern recognition receptors, especially Toll-like receptors (TLRs) and RIG-I-like receptors (RLRs) (Kawai and Akira, 2010; Chen et al., 2013). When activated by viral nucleic acids, TLRs and RLRs will activate the TBK1–IRF3 axis, leading to type I interferon (IFN) expression and secretion (Garcia-Sastre and Biron, 2006; He et al., 2017). Then, the released IFNs induce hundreds of interferon-stimulated genes (ISGs) via the Janus kinase-signal transducer and activator of transcription (JAK–STAT) signaling pathway to clear the invaded virus (Platanias, 2005; Garcia-Sastre and Biron, 2006; Shu et al., 2015). Among them, the double-stranded RNA-dependent protein kinase PKR, the myxovirus resistance gene Mx, the 2′-5′ oligoadenylate synthetases, and interferon induced transmembrane protein 3 (IFITM3) have been shown to disrupt viral infection in various manners (Garcia et al., 2006; Rafique et al., 2011; Liu et al., 2013). More than 350 genes have been characterized as ISGs. However, their roles and mechanisms in fighting against multiple distinct classes of viruses remain largely unexplored.

Purinergic signaling and purinergic receptors are important in both innate and adaptive immune responses. Purinergic signaling was first reported in 1929 and, after several decades of study, many of the biologic effects of ATP, UTP, ADP, UDP, and adenosine signaling were discovered (Eltzschig et al., 2012; Idzko et al., 2014). In tissue injury or pathogen infection, nucleotides can be released from stressed cells as a danger signal, alerting the cells by interaction with purinergic receptors in an autocrine or paracrine manner (Cho et al., 2014). Nineteen different purinergic receptor subtypes have been identified, which can be classified into P1 and P2 receptors. Four P1 receptor subtypes can be activated by adenosine. P2 receptors can be further divided into P2Y receptors (P2YRs) and P2X receptors (P2XRs) based on their structures and distinct signal-transduction mechanisms. P2YRs are G-protein-coupled receptors

Received November 28, 2017. Revised May 16, 2018. Accepted August 20, 2018.

for ATP, ADP, UTP, and UDP, while P2XRs are nucleotide-gated ion channels and can be activated by ATP (Ralevic and Burnstock, 1998; Junger, 2011; Idzko et al., 2014). Many studies revealed crucial roles for P2 receptors during inflammatory and infectious diseases. For example, ATP-triggered P2X7 activation is crucial for the activation of NLRP3 inflammasome and the subsequent release of interleukin-1β (Di Virgilio et al., 2017). ATP/UTP receptor $P2Y_2$ signaling has been identified as a 'find-me' signal to recruit motile phagocytes, thereby promoting clearance of apoptotic cells or bacteria (Elliott et al., 2009; Chen et al., 2010). Our previous study demonstrated that the ADP-mediated $P2Y_{12}$/$P2Y_{13}$ signal pathway protects the host defense against bacterial infection via ERK signaling (Zhang et al., 2018). However, whether ADP- (or its receptors-) mediated immune regulation is also involved in viral infection remains unclear.

$P2Y_1$, $P2Y_{12}$, and $P2Y_{13}$ are all receptors for ADP. $P2Y_1$ binds to GTP-binding protein subunit alpha q (Gq), which can evoke calcium signaling. While $P2Y_{12}$ and $P2Y_{13}$ interact with GTP-binding protein subunit alpha i (Gi), which can suppress the activity of adenylate cyclase (ADCY) and the production of cyclic adenosine monophosphate (cAMP) (Zhang et al., 2015; Shinozaki et al., 2017). In this study, we demonstrate that $P2Y_{13}$, as an ISG, and its ligand, ADP, is released from infected cells as a danger signal during viral infection, which restricts the replication of both DNA and RNA viruses. ADP/$P2Y_{13}$-mediated protection against viral infection operates by suppressing the expression of exchange protein activated by cAMP 1 (EPAC1), which is an alternative key intracellular sensor for cAMP. Therefore, we demonstrated that ADP/$P2Y_{13}$ restricts viral infection through suppressing the cAMP/EPAC1 signaling pathway, which has potential therapeutic significance in the prevention and control of viral diseases.

Results

The expression of $P2Y_{13}$ is increased by IFN through JAK/STAT pathway

To identify P2Y family members potentially involved in antiviral immune responses, we treated mouse bone marrow-derived macrophages (BMDMs) with IFN-α, IFN-β, and IFN-γ to appraise the RNA expression of all P2Y family members by quantitative real-time PCR (Q-PCR). As shown in Figure 1A, the RNA expression of $P2Y_{13}$ was upregulated obviously by all three IFNs. The protein level of $P2Y_{13}$ also upregulated by IFN-β (Figure 1B). Besides, when blocked IFN receptor (IFNAR) with the anti-IFNAR antibody, the upregulated expression of $P2Y_{13}$ was decreased (Figure 1C), suggesting that $P2Y_{13}$ upregulation is dependent on signals downstream of IFN. The JAK/STAT pathway is crucial for IFN-induced cellular antiviral signaling. To determine whether IFN-induced $P2Y_{13}$ upregulation via the JAK/STAT1 pathway, we pretreated mouse peritoneal macrophages (PEMs) with ruxolitinib (a JAK1 inhibitor) and fludarabine (a STAT1 inhibitor) and found that IFNβ-induced $P2Y_{13}$ expression was blocked by both inhibitors (Figure 1D and E). Inhibition of STAT1 also reduced VSV-induced $P2Y_{13}$ expression (Figure 1F). In addition, knockout of TLR3 to block TLR3-mediated activation of IFN also suppressed poly(I:C)-induced $P2Y_{13}$ expression (Figure 1G). Taken together, these data demonstrated that $P2Y_{13}$ has the typical characteristics of ISGs.

Extracellular ADP protects cell lines from viral infection

As an endogenous ligand to purinergic receptors, ADP can be released from injured cells to activate $P2Y_1$, $P2Y_{12}$, and $P2Y_{13}$ receptors. To investigate the potential role of ADP as a danger signal in viral infection, the release of endogenous ADP in viral-infected cells was measured. As shown in Figure 2A and B, extracellular ADP in VSV-infected cell supernatant was clearly increased in a time-dependent manner. Besides, NDV-infected BMDMs and HSV-1-infected HEK293T cells also release large amounts of ADP (Figure 2C and Supplementary Figure S1A), suggesting ADP can be released as a danger signal during viral infection. To investigate the biological significance of ADP, we pretreated the cells with ADP before VSV infection. To our surprise, the RNA replication of VSV in ADP-treated RAW264.7 cells was reduced significantly in a time- (Figure 2D) and concentration- (Figure 2E) dependent manner. Accordingly, the viability of VSV-infected RAW 264.7 cells was increased dramatically by ADP in a concentration-dependent manner while have little influence on uninfected cells (Figure 2F and Supplementary Figure S1B), indicating that extracellular ADP protects cells from VSV infection. To confirm whether ADP has broad-spectrum antiviral activities, RAW264.7 cells and BMDMs were pretreated with ADP before VSV, NDV, and HSV-1 infection. As shown in Figure 2G–J and Supplementary Figure S1C, the RNA expression of VSV, NDV, HSV-1 and the titers of VSV were all strikingly decreased by ADP. Similar results were observed in HEK293T cells, where cell cytopathic effects were induced by VSV and HSV-1, as determined using a crystal violet staining assay (Supplementary Figure S1D and E). We further infected HEK293T and Hela cells with VSV-GFP and MLV-GFP and found that the number of GFP-positive cells was decreased in ADP-treated cells, indicating that VSV-GFP and MLV-GFP were restricted by ADP (Supplementary Figure S1F–I). To rule out the possibility that ADP degradation products mediate the suppression of viral replication, we treated cells with non-hydrolyzable ADP analog ADP-β-s. As shown in Supplementary Figure S1J, ADP-β-s has a similar role as ADP in restricting VSV replication. Taken together, our data suggested that extracellular ADP has broad-spectrum antiviral activities, which have great potential in protecting hosts from a viral infection.

$P2Y_{13}$ deficiency leads to susceptibility to viral infection

To explore the key receptors involved in ADP-mediated antiviral activities, we detected the expression of $P2Y_1$, $P2Y_{12}$, and $P2Y_{13}$ after VSV infection. As shown in Figure 3A, only the expression of $P2Y_{13}$ was increased significantly, whereas the expression of $P2Y_1$ and $P2Y_{12}$ was little changed in VSV-infected RAW264.7 cells. Similar data were observed in poly(I:C)-treated BMDMs (Figure 3B). We then used MRS 2179 and MRS 2211 to inhibit $P2Y_1$ and P2Y13, respectively, to verify whether $P2Y_1$ and $P2Y_{13}$ contributed to ADP-mediated antiviral activities. We found that ADP-mediated antiviral activities were little influenced by

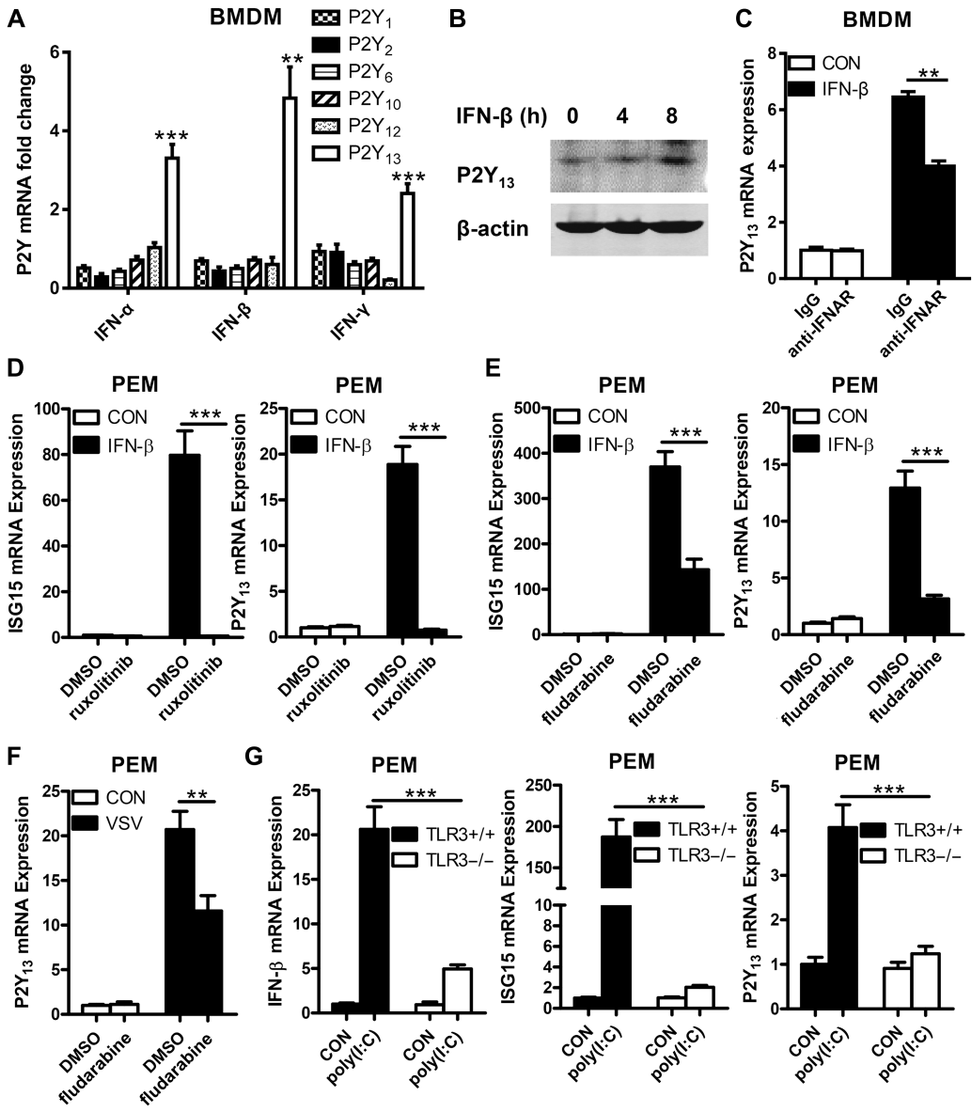

Figure 1 IFN signal pathway increases P2Y$_{13}$ expression. (**A**) Mouse BMDMs were treated with IFN-α, IFN-β, or IFN-γ (100 ng/ml) for 2 h, and mRNA expression of P2Y family was detected by Q-PCR. (**B**) Mouse PEMs were treated with IFN-β (100 ng/ml) for 4 or 8 h, and the expression of P2Y$_{13}$ protein was detected by western blotting. (**C**) Mouse BMDMs were pretreated or not with anti-IFN-α/β receptor IgG (10 μg/ml) for 4 h before being treated with IFN-β (100 ng/ml) for 4 h, and the expression of P2Y$_{13}$ mRNA was detected by Q-PCR. (**D**) Mouse PEMs were pretreated or not with Ruxolitinib (10 μg/ml) for 1 h and then stimulated with IFN-β (100 ng/ml) for 4 h. The expression of ISG15 and P2Y$_{13}$ mRNA was detected by Q-PCR. (**E**) Mouse PEMs were pretreated with or without fludarabine (100 μg/ml) for 30 min and then stimulated with IFN-β (100 ng/ml) for 4 h. The expression of ISG15 and P2Y$_{13}$ mRNA was detected by Q-PCR. (**F**) Mouse PEMs were pretreated or not with fludarabine (100 μg/ml) for 30 min and then infected with VSV (MOI = 1) for 12 h. The expression of P2Y$_{13}$ mRNA was detected by Q-PCR. (**G**) TLR3$^{+/+}$ and TLR3$^{-/-}$ mouse PEMs were treated with poly(I:C) (20 μg/ml) for 4 h. The expression of IFN-β, ISG15, and P2Y$_{13}$ mRNA was detected by Q-PCR. Data are shown as mean ± SD. $^{**}P < 0.01$; $^{***}P < 0.001$.

MRS 2179 but significantly decreased by MRS 2211 as shown in Figure 3C–F, and both of MRS 2179 and MRS 2211 have little influence on cell viability (Supplementary Figure S2A and B). Consistently, when infected wild-type, P2Y$_1$-, P2Y$_{12}$-, and P2Y$_{13}$-deficient BMDMs with VSV, the VSV RNA replication was increased only in P2Y$_{13}$-deficient BMDMs, not in P2Y$_1$- or P2Y$_{12}$-knockout BMDMs (Figure 3G). Meanwhile, ADP-reduced VSV RNA replication was compensated in P2Y$_{13}$-deficient PEMs (Figure 3H). Furthermore, the protein expression of vesicular stomatitis virus glycoprotein (VSV-G) was significantly increased in P2Y$_{13}$-deficient PEMs and overexpression of P2Y$_{13}$ in HeLa cells significantly repressed VSV replication (Figure 3I; Supplementary

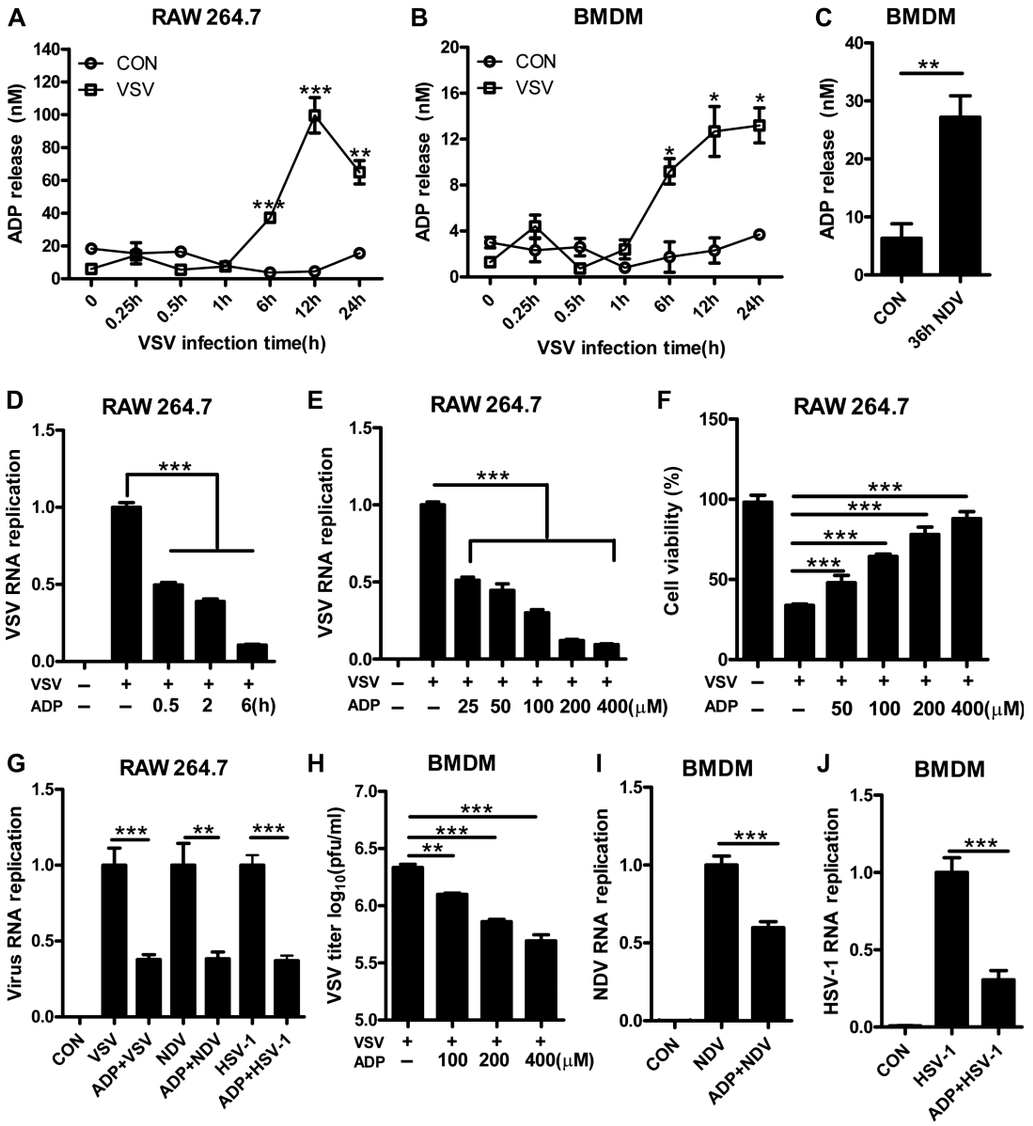

Figure 2 ADP protects cell lines against virus infection. (**A**) RAW264.7 cells were infected with VSV (MOI = 0.01), and then the levels of ADP release were measured over time. (**B**) Mouse BMDMs were infected with VSV (MOI = 1), and the levels of extracellular ADP were measured over time. (**C**) Mouse BMDMs were infected with NDV (MOI = 0.1) for 36 h, and then the levels of ADP release were measured. (**D**) RAW264.7 cells were treated with ADP (100 μM) for various periods and then infected with VSV (MOI = 0.01) for 12 h. Intracellular VSV RNA replicates were detected by Q-PCR. (**E**) RAW264.7 cells were treated with various concentrations of ADP for 6 h and then infected with VSV (MOI = 0.01) for 12 h. VSV RNA replicates were detected by Q-PCR. (**F**) RAW264.7 cells were pretreated with various concentrations of ADP for 6 h and then infected with VSV (MOI = 0.01) for 24 h. Cell viability was detected by MTS assay. (**G**) RAW264.7 cells were treated with ADP (100 μM) for 6 h and then infected with VSV (MOI = 0.01), NDV (MOI = 0.01), and HSV-1 (MOI = 0.01) for 12 h. Virus RNA replicates were detected by Q-PCR. (**H**) Mouse BMDMs were treated with various concentrations of ADP for 6 h and then infected with VSV (MOI = 1) for 12 h. VSV titers in supernatants were measured by plaque assay. (**I** and **J**) Mouse BMDMs were treated with ADP (100 μM) for 6 h and then infected with NDV (MOI = 0.1) and HSV-1 (MOI = 0.1) for 24 h Virus RNA replicates were detected by Q-PCR. Data are shown as mean ± SD. $^{*}P < 0.05$; $^{**}P < 0.01$; $^{***}P < 0.001$.

Figure S2C and D). Taken together, our data suggested that $P2Y_{13}$ deficiency facilitates VSV infection and ADP-mediated antiviral activities primarily through the $P2Y_{13}$ receptor.

ADP/$P2Y_{13}$ protects mice from viral infection

To further confirm the *in vivo* antiviral activities of ADP/$P2Y_{13}$, we challenged wild-type and $P2Y_{13}$-deficient mice with a lethal

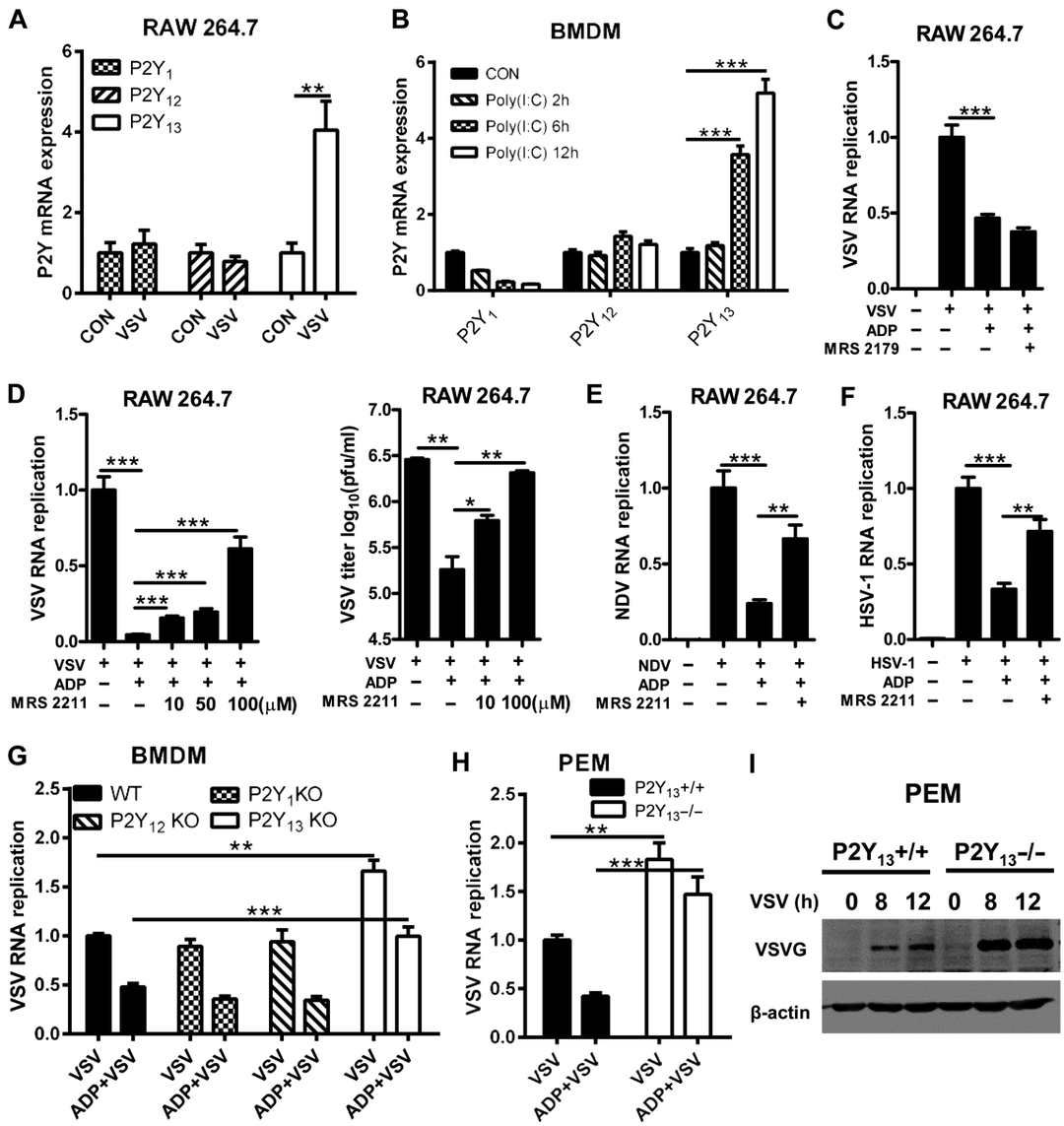

Figure 3 ADP-mediated antiviral activities are dependent on P2Y$_{13}$. (**A**) RAW264.7 cells were infected with VSV (MOI = 0.01) or not for 2 h. P2Y$_1$, P2Y$_{12}$, and P2Y$_{13}$ mRNA expression levels were detected by Q-PCR. (**B**) Mouse BMDMs were stimulated with poly(I:C) (20 μg/ml) for the indicated time, and then P2Y$_1$, P2Y$_{12}$, and P2Y$_{13}$ mRNA expression levels were detected by Q-PCR. (**C**) RAW264.7 cells were treated with MRS 2179 (10 μM) for 30 min before being treated with ADP (100 μM) for 6 h. The cells were then infected with VSV (MOI = 0.01) for 12 h, and VSV RNA replicates were detected by Q-PCR. (**D**) RAW264.7 cells were pretreated or not with various concentrations of MRS 2211 for 1 h before being treated with ADP (100 μM) for 6 h. The cells were then infected with VSV (MOI = 0.01) for 12 h. VSV RNA replicates were detected by Q-PCR and VSV titers in supernatants were measured by plaque assay. (**E** and **F**) RAW264.7 cells were pretreated or not with MRS 2211 (50 μM) for 1 h before being treated with ADP (100 μM) for 6 h. The cells were then infected with NDV (MOI = 0.01) and HSV-1 (MOI = 0.01) for 16 h, and virus RNA replicates were detected by Q-PCR. (**G**) WT, P2Y$_1{}^{-/-}$, P2Y$_{12}{}^{-/-}$, and P2Y$_{13}{}^{-/-}$ mouse BMDMs were treated with ADP (100 μM) for 6 h and then infected with VSV (MOI = 1) for 12 h. VSV RNA replicates were detected by Q-PCR. (**H**) P2Y$_{13}{}^{+/+}$ and P2Y$_{13}{}^{-/-}$ PEMs were treated with ADP (100 μM) for 6 h. The cells were then infected with VSV (MOI = 1) for 12 h, and VSV RNA replicates were detected by Q-PCR. (**I**) P2Y$_{13}{}^{+/+}$ and P2Y$_{13}{}^{-/-}$ PEMs were infected with VSV for the indicated time, and the VSV-G protein expression levels were detected by western blotting. Data are shown as mean ± SD. *$P < 0.05$; **$P < 0.01$; ***$P < 0.001$.

dose of VSV. As shown in Figure 4A, the survival of ADP-treated wild-type mice was increased obviously, but there was little change in that of P2Y$_{13}$-deficient mice. P2Y$_{13}$-deficient mice were more susceptible to VSV infection. On the other hand, if we intraperitoneally injected mice with ADP to activate P2Y$_{13}$, VSV distributions in the liver, spleen, and lung were all significantly

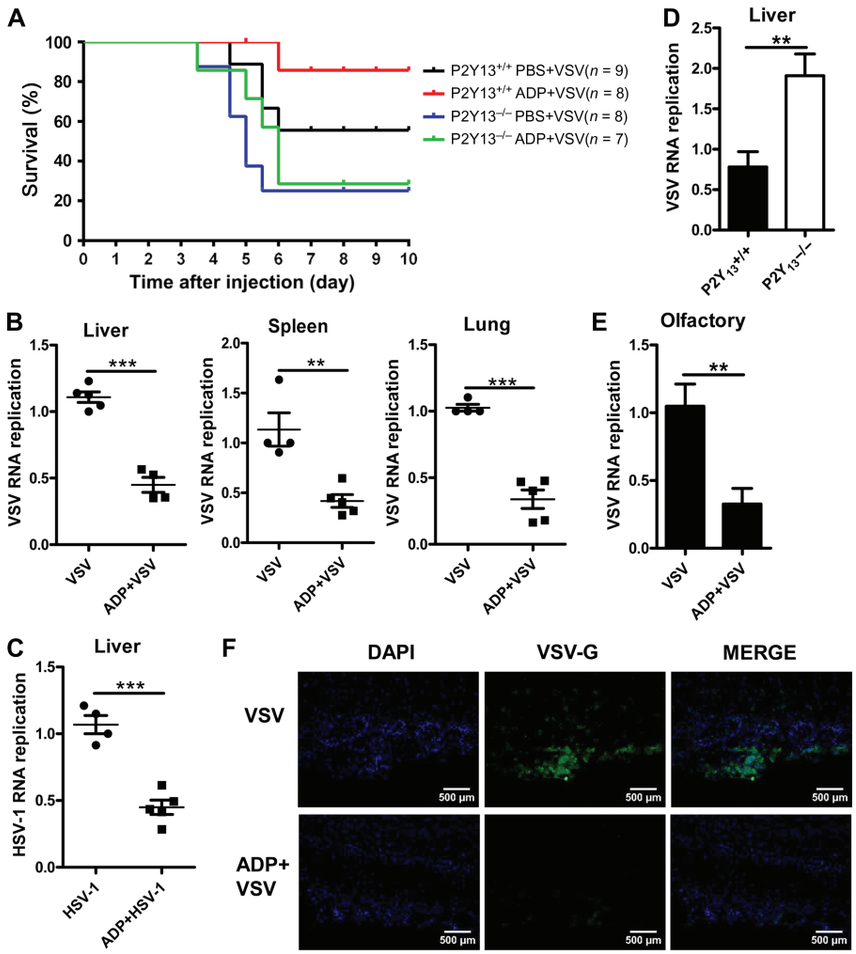

Figure 4 ADP/$P2Y_{13}$ protects mice against virus infection. (**A**) Eight-week-old $P2Y_{13}^{+/+}$ or $P2Y_{13}^{-/-}$ mice were intraperitoneally treated with ADP (50 mg/kg) for 6 h and then intraperitoneally injected with VSV (1×10^8 pfu/g). Mice were executed for 5 days and mouse survival was recorded for 10 days. (**B**) Six-week-old mice were intraperitoneally treated with ADP (50 mg/kg) for 6 h and then intraperitoneally injected with VSV (1×10^8 pfu/g) for 24 h. VSV RNA replicates in organs were detected by Q-PCR. (**C**) Six-week-old mice were intraperitoneally treated with ADP (50 mg/kg) for 6 h and then intraperitoneally injected with HSV-1 (1×10^7 pfu/g) for 36 h. HSV-1 RNA replicates in livers were detected by Q-PCR. (**D**) Eight-week-old $P2Y_{13}^{+/+}$ or $P2Y_{13}^{-/-}$ mice were intraperitoneally injected with VSV (1×10^8 pfu/g) for 24 h and VSV RNA replicates in livers were detected by Q-PCR. (**E**) Six-week-old mice were treated with ADP (5 mg/kg) through nasal dropping for 6 h and then intranasally infected with VSV (1×10^8 pfu/g) for 24 h. VSV RNA replicates in olfactory tissues were detected by Q-PCR. (**F**) Six-week-old mice were treated as in **E**, and VSV invaded in olfactory tissues were detected by immunofluorescence. Scale bar, 500 μm. Data are shown as mean ± SD. $^{**}P < 0.01$; $^{***}P < 0.001$.

decreased (Figure 4B). Similar data were observed during HSV-1 infection (Figure 4C). Besides, more VSV RNA replicates were found in $P2Y_{13}$-deficient mice liver (Figure 4D). As a neurotropic virus, VSV can invade the nervous system and is transmitted directly via the transcutaneous or transmucosal route. Thus, to mimic the natural infection of VSV, we treated mice with ADP through nasal dripping and then intranasally infected with VSV. As shown in Figure 4E and F, VSV RNA replication and VSV-G in olfactory bulbs were both significantly reduced by ADP. Taken together, these data demonstrated that ADP/$P2Y_{13}$ plays an important role in protecting mice from VSV infection, suggesting that ADP/$P2Y_{13}$ has potential as a novel antiviral drug target.

ADP/$P2Y_{13}$ restricts viral replication by inhibiting cAMP signaling

Type I IFN plays pivotal roles in fighting against the invaded virus, so we tested whether it was involved in ADP/$P2Y_{13}$-mediated antiviral activities. However, when we treated BMDMs with ADP, the RNA expression of IFN-α and IFN-β was little changed (Supplementary Figure S3A and B). $P2Y_{13}$ signaling can suppress the activity of ADCY and the production of cAMP. To confirm that, RAW264.7 cells were pretreated or not with MRS 2211 before being treated with ADP. As shown in Figure 5A, ADP significantly suppressed the production of cAMP, while $P2Y_{13}$ antagonist MRS 2211 rescued this phenomenon.

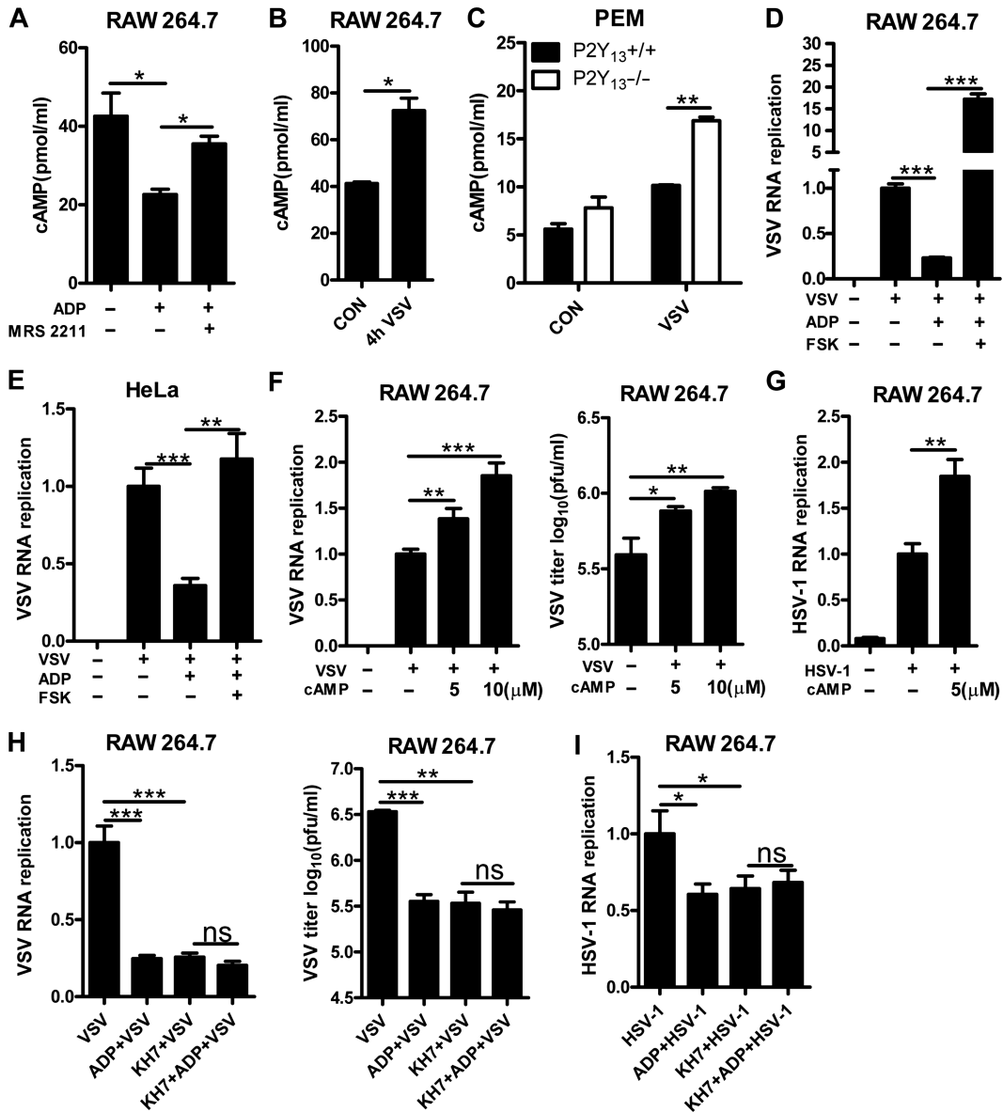

Figure 5 cAMP is involved in ADP-mediated antiviral activities. (**A**) RAW264.7 cells were pretreated or not with MRS 2211 (50 μM) for 1 h before being treated with ADP (100 μM) for 2 h, and intracellular cAMP was detected by ELISA. (**B**) RAW264.7 cells were infected with VSV (MOI = 0.01) for 4 h, and intracellular cAMP was detected by ELISA. (**C**) P2Y$_{13}$$^{+/+}$ or P2Y$_{13}$$^{-/-}$ mouse PEMs were infected with VSV (MOI = 1) for 4 h, and intracellular cAMP was detected by ELISA. (**D**) RAW264.7 cells were treated with forskolin (100 μM) for 1 h before a 6-h ADP (100 μM) treatment and then infected with VSV (MOI = 0.01) for 12 h. Intracellular VSV RNA replicates were detected by Q-PCR. (**E**) Hela cells were treated with forskolin (50 μM) for 1 h before a 6-h ADP (100 μM) treatment and then infected with VSV (MOI = 0.01) for 12 h. Intracellular VSV RNA replicates were detected by Q-PCR. (**F**) RAW264.7 cells were treated with cAMP (5 or 10 μM) for 6 h and then infected with VSV (MOI = 0.01) for 12 h. VSV RNA replicates were detected by Q-PCR and VSV titers in supernatants were measured by plaque assay. (**G**) RAW264.7 cells were treated with cAMP (5 μM) for 6 h and then infected with HSV-1 (MOI = 0.01) for 16 h. HSV-1 RNA replicates were detected by Q-PCR. (**H**) RAW264.7 cells were pretreated or not with KH7 (10 μM) for 1 h before being treated with ADP (100 μM) for 6 h. The cells were then infected with VSV (MOI = 0.01) for 12 h. VSV RNA replicates were detected by Q-PCR and VSV titers in supernatants were measured by plaque assay. (**I**) RAW264.7 cells were pretreated or not with KH7 (10 μM) for 1 h before being treated with ADP (100 μM) for 6 h. The cells were then infected with HSV-1 (MOI = 0.01) for 16 h, and HSV-1 RNA replicates were detected by Q-PCR. Data are shown as mean ± SD. *$P < 0.05$; **$P < 0.01$; ***$P < 0.001$; ns, not significant.

However, to our surprise, VSV infection caused an obvious increase in cellular cAMP levels (Figure 5B). Besides, P2Y$_{13}$-deficient PEMs showed higher cellular cAMP levels than wild-type PEMs during VSV infection (Figure 5C). So, we examined the role of cAMP in ADP/P2Y$_{13}$-mediated antiviral activities. We first found that ADCY activator forskolin blocked ADP-mediated

antiviral activity completely (Figure 5D and E). Furthermore, cAMP treatment promoted viral replication obviously and also rescued the ADP-reduced cell cytopathic effects and VSV replication (Figure 5F and G; Supplementary Figure S3C and D). Consistent with this, KH7 (a selective inhibitor of ADCY) treatment significantly inhibited cell cytopathic effects and VSV replication (Supplementary Figure S3E and F). ADP-mediated antiviral activities were also significantly blocked by KH7 (Figure 5H and I). The cell viability assays revealed that these phenomena were not caused by the toxicity of forskolin, cAMP, and KH7 (Supplementary Figure S3G–I). Taken together, these results suggested that cAMP plays a key role in ADP/$P2Y_{13}$-mediated antiviral activities.

ADP/$P2Y_{13}$ restricts viral replication in an EPAC1-dependent manner

When intracellular cAMP is increased by upstream signaling, EPAC and protein kinase A (PKA) could be activated as classical sensors for cAMP. Thus, we treated HeLa cells with ESI-09 (EPAC1/2 inhibitor), HJC0350 (EPAC2 selective inhibitor), and H89 (PKA inhibitor) at a safety concentration (Supplementary Figure S4A–C). As shown in Supplementary Figure S4D, the replication of VSV is dramatically suppressed by both ESI-09 and H89, but not HJC0350, suggesting that EPAC1 and PKA may be involved in ADP/$P2Y_{13}$-mediated restriction to VSV. However, when we inhibited PKA with H89, the replication of VSV (Figure 6A) and HSV-1 (Figure 6B) in HeLa cells are still suppressed by ADP, whereas ADP-reduced VSV, HSV-1, and NDV replication was significantly blocked by ESI-09, but not HJC0350 (Figure 6C–F and Supplementary Figure S4E). Besides, the ADP-reduced VSV-G expression was also blocked by ESI-09 (Figure 6G). These data show that EPAC1 is crucial in ADP/$P2Y_{13}$-mediated antiviral activities. In addition, we generated an EPAC1-knockout cell line using the CRISPR/Cas9 system (Figure 6H). As shown in Figure 6I and J, when EPAC1 is deficient, ADP-mediated suppression of VSV RNA replication and VSV-G expression were eliminated. Taken together, these results demonstrated that ADP/$P2Y_{13}$-mediated antiviral activities are dependent on EPAC1. Inhibiting EPAC1 with ESI-09 in RAW264.7 cells significantly suppressed VSV and HSV-1 replication, and EPAC1 knockout also inhibited HSV-1 replication, demonstrating that either inhibition or deletion of EPAC1 has broad-spectrum antiviral activities (Supplementary Figure S4F–H).

ADP inhibits viral replication via suppressing EPAC1 expression

To further confirm the key role of EPAC1 in viral infection, we detected the expression of EPAC1 in viral-infected cells. As shown in Figure 7A, when infected RAW264.7 cells with VSV, NDV, and HSV-1, RNA expression of EPAC1 was increased significantly. Deficiency in $P2Y_{13}$ maintained higher expression of EPAC1 in PEMs after infection with VSV (Figure 7B). In addition, the expression of EPAC1 protein also upregulated after virus infection as shown in Figure 7C and Supplementary Figure S5A, B. However, to our surprise, the increased expression of EPAC1 induced by VSV was reduced by ADP in a dose-dependent manner (Supplementary Figure S5C and D). To exclude that the downregulation of EPAC1 may be due to the attenuation of VSV replication by ADP, cell lines were only treated with ADP. As shown in Figure 7D–F and Supplementary Figure S5E, the endogenous RNA expression of EPAC1 was directly inhibited by ADP. The protein expression of EPAC1 was also inhibited by ADP (Figure 7G and H). Taken together, these data demonstrated that the virus-increased EPAC1 expression is suppressed by ADP, which restricts the viral infection in host cells.

Discussion

$P2Y_{12}$ and $P2Y_{13}$, as membrane receptors for ADP, are both Gi-coupled receptors that inhibit the activity of ADCY and reduce the production of cAMP (Vitiello et al., 2012). $P2Y_{12}$ is highly expressed in platelets and plays a central role in platelet activation, which has become a drug target for atherothrombotic diseases, whereas $P2Y_{13}$ is mainly expressed in the bone marrow, spleen, liver, and brain (Savi et al., 2006; Vitiello et al., 2012). Previous studies have shown that $P2Y_{12}$ and $P2Y_{13}$ are both involved in the development of pain behavior during nerve injury and the expression of pro-inflammatory cytokines (Kobayashi et al., 2012; Liu et al., 2017). However, the role of $P2Y_{12}$ and $P2Y_{13}$ receptors in viral infection remains unclear. Here we demonstrate that $P2Y_{13}$ is upregulated by type I IFN ($P2Y_{12}$ is little changed) and its endogenous ligand, ADP, is released as danger signals from virus-infected cells. Consequently, extracellular ADP-activated $P2Y_{13}$ protects the host against viral infection in a cAMP-dependent manner. Thus, our study reveals an important role of ADP/$P2Y_{13}$ in fighting against viral infection, which demonstrates the potential of purinergic receptors as novel antiviral targets.

Upon viral infection, the host initiates a series of signaling cascades to induce the production of type I IFN, which results in the induction of ISGs to exclude invaded virus (Ooi et al., 2014; Zhan et al., 2015). Previous studies reported that ISGs could further promote the production of type I IFN to eliminate the virus, such as ISG15 and IFIT3 (Lu et al., 2006; Liu et al., 2011). Therefore, we tested whether ADP/$P2Y_{13}$ influences the expression of type I IFN. Our results show that ADP enhanced IFN expression by only a little. Because ADP clearly inhibited virus replication, we hypothesized that there must be another way for ADP/$P2Y_{13}$ to restrict viral infection. Thus, the classic Gi-coupled signaling pathway came to mind. Interestingly, we found that ADP-inhibited VSV replication and cell cytopathic effects were rescued by both ADCY activator forskolin and cAMP. Moreover, similar to ADP, the ADCY inhibitor KH7 also inhibited VSV replication, suggesting that cAMP plays a key role in ADP/$P2Y_{13}$-mediated antiviral activities.

As the first identified second messenger, cAMP plays a crucial role in microbial pathogenesis (McDonough and Rodriguez, 2011). PKA and EPAC are the two classical sensors for intracellular cAMP, which are essential for many biological processes (Gloerich and Bos, 2010). PKA plays important roles in metabolism, cell cycle, cell migration, differentiation, and apoptosis (Yan et al., 2017). Previous studies have reported that PKA can inhibit IFN induction of the JAK/STAT pathway (David et al., 1996). Recently, a new study reported that PKA catalytic (PKAC)

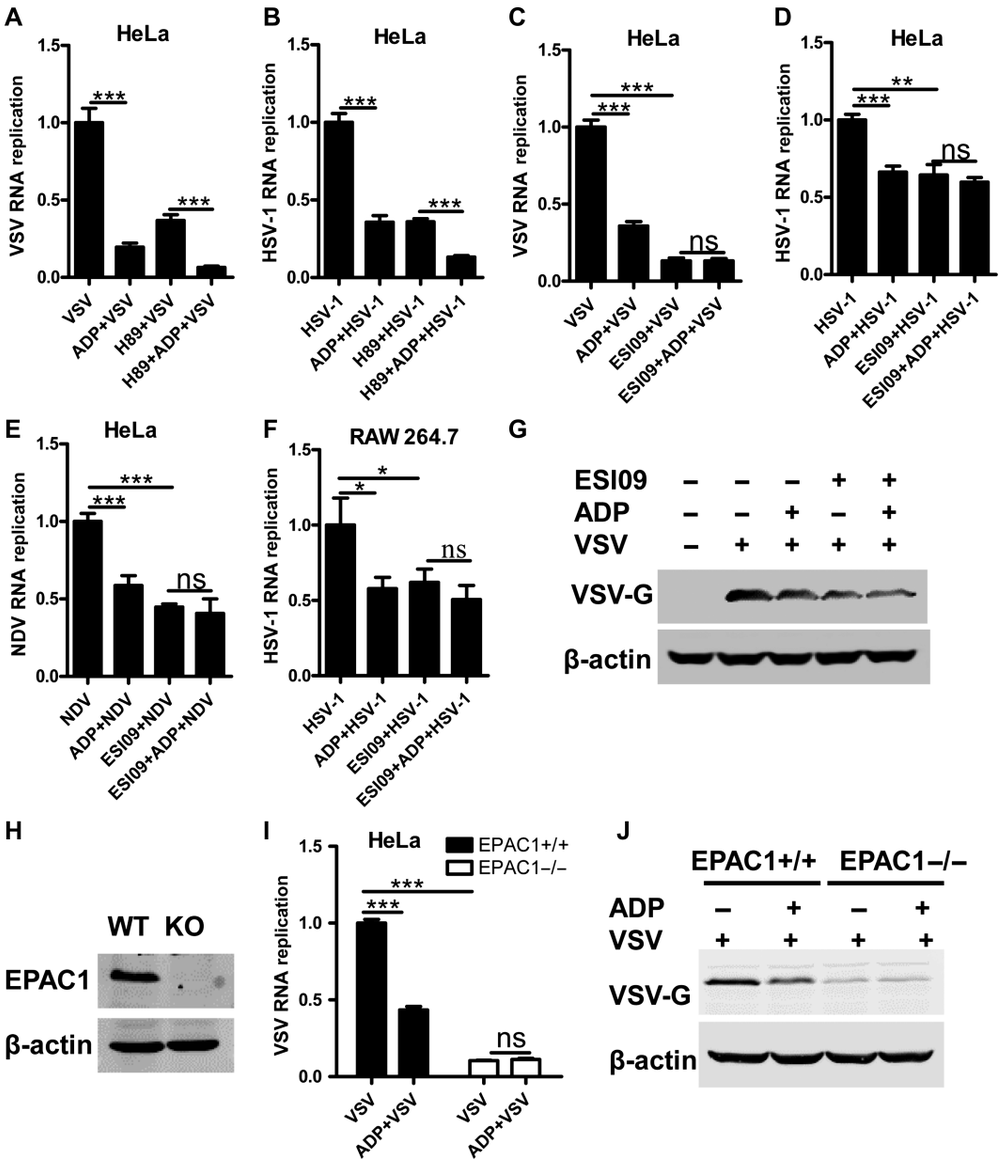

Figure 6 ADP-mediated antiviral activities are dependent on EPAC1. (**A**) HeLa cells were treated or not with H89 (10 μM) for 1 h before being treated with ADP (100 μM) for 6 h and then infected with VSV (MOI = 0.01) for 12 h. VSV RNA replicates were detected by Q-PCR. (**B**) HeLa cells were treated or not with H89 (10 μM) for 1 h before being treated with ADP (100 μM) for 6 h and then infected with HSV-1 (MOI = 0.01) for 16 h. HSV-1 RNA replicates were detected by Q-PCR. (**C**) HeLa cells were pretreated or not with ESI-09 (10 μM) for 1 h before being exposed to ADP (100 μM) for 6 h. The cells were then infected with VSV (MOI = 0.01) for 12 h and VSV RNA replicates were detected by Q-PCR. (**D** and **E**) HeLa cells were pretreated or not with ESI-09 (10 μM) for 1 h before being exposed to ADP (100 μM) for 6 h. The cells were then infected with HSV-1 (MOI = 0.01) or NDV (MOI = 0.01) for 16 h and viral RNA replicates were detected by Q-PCR. (**F**) RAW264.6 cells were treated or not with ESI-09 (10 μM) for 1 h before being exposed to ADP (100 μM) for 6 h. The cells were then infected with HSV-1 (MOI = 0.01) for 16 h, and HSV-1 RNA replicates were detected by Q-PCR. (**G**) HeLa cells were pretreated or not with ESI-09 (10 μM) for 1 h before being exposed to ADP (100 μM) for 6 h. The cells were then infected with VSV (MOI = 0.01) for 12 h and VSV-G protein levels were detected by western blotting. (**H**) EPAC1$^{+/+}$ and EPAC1$^{-/-}$ HeLa cells were exposed to VSV (MOI = 0.01) for 12 h, and the expression of EPAC1 was detected by western blotting. (**I**) EPAC1$^{+/+}$ and EPAC1$^{-/-}$ HeLa cells were treated with ADP (100 μM) for 6 h and then infected with VSV (MOI = 0.01) for 12 h. VSV RNA replicates were detected by Q-PCR. (**J**) EPAC1$^{+/+}$ and EPAC1$^{-/-}$ HeLa cells were treated with ADP (100 μM) for 6 h and infected with VSV (MOI = 0.01) for 12 h. VSV-G protein levels were detected by western blotting. Data are shown as mean ± SD. *$P < 0.05$; **$P < 0.01$; ***$P < 0.001$; ns, not significant.

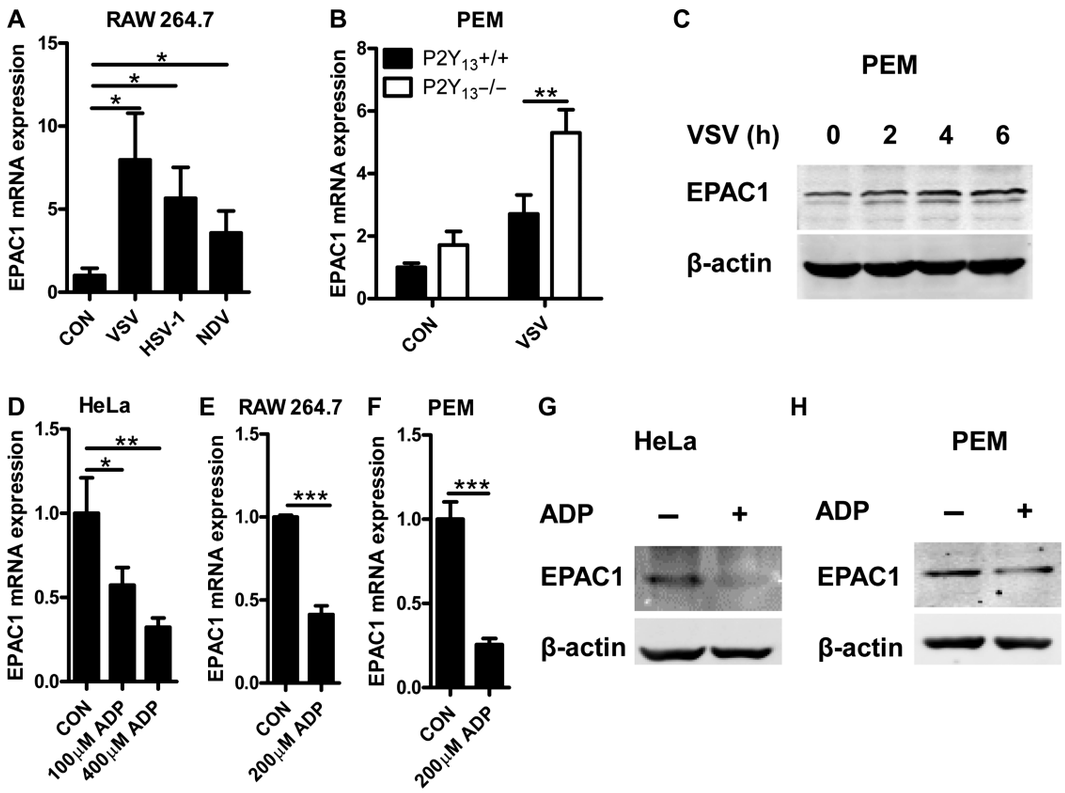

Figure 7 ADP inhibits EPAC1 expression. (**A**) RAW264.7 cells were infected with VSV (MOI = 0.01), NDV (MOI = 0.01), and HSV-1 (MOI = 0.01) for 12 h. EPAC1 mRNA levels were detected by Q-PCR. (**B**) $P2Y_{13}^{+/+}$ or $P2Y_{13}^{-/-}$ mouse PEMs were infected with VSV (MOI = 1) for 2 h. EPAC1 mRNA levels were detected by Q-PCR. (**C**) Mouse PEMs were infected with VSV (MOI = 1) for the indicated time, and EPAC1 protein levels were detected by western blotting. (**D**) HeLa cells were treated with 100 μM or 400 μM ADP for 2 h and EPAC1 mRNA levels were detected by Q-PCR. (**E** and **F**) RAW264.7 cells and mouse PEMs were treated with ADP (200 μM) for 2 h. EPAC1 mRNA levels were detected by Q-PCR. (**G** and **H**) HeLa cells and mouse PEMs were treated with ADP (400 μM) for 8 h. EPAC1 protein levels were detected by western blotting. Data are shown as mean ± SD. *$P < 0.05$; **$P < 0.01$; ***$P < 0.001$.

subunits α and β could negatively regulate RNA virus-triggered signaling and ultimately attenuate the innate antiviral response (Yan et al., 2017). EPAC has two isoforms, EPAC1 and EPAC2. The cAMP/EPAC signal pathway is important for controlling various cellular functions, including cell adhesion, exocytosis, and microtubule dynamics. Previous studies have reported that EPAC1 is a potential target for the treatment of fatal rickettsioses and that the silencing of EPAC1 gene expression renders cells resistant to MERS-CoV infection (Gong et al., 2013; Tao et al., 2014). In our study, we found that both PKA and EPAC inhibitors suppress viral replication. However, only EPAC inhibition could block ADP/$P2Y_{13}$-mediated antiviral activities. Also, we found that the EPAC2 inhibitor could not block ADP/$P2Y_{13}$-mediated antiviral activities. These findings suggest that ADP/$P2Y_{13}$-mediated antiviral activities are mainly dependent on EPAC1. Knockout of EPAC1 in HeLa cells showed similar results and further proved this point. Taken together, our results showed that, upon viral infection, the virus can trigger an upregulation of intracellular cAMP levels to activate EPAC1 and thereby facilitating virus replication. However, the virus also triggers ADP released from these cells, which will activate $P2Y_{13}$ and suppress the cAMP/EPAC1 signal pathway to restrain virus replication. This phenomenon revealed a negative feedback regulation in animals during viral infection, and that activation of $P2Y_{13}$ and inhibition of the cAMP/EPAC1 signal pathway are potential antiviral strategies.

Materials and methods

Mice

$P2Y_1$, $P2Y_{12}$, and $P2Y_{13}$ knockout mice were described previously (Zhang et al., 2018). TLR3 knockout mice were a gift from professor Yuping Lai (East China Normal University) and were described previously (Wu et al., 2016). C57BL/6 wild-type mice were purchased from the Shanghai Laboratory Animal Company. All of the mice were maintained in specific pathogen-free (SPF) facilities at the Animal Center of East China Normal University. All animal experiments were done following institutional guidelines.

Reagents

ADP, ADP-β-s, MRS 2179, Forskolin, cAMP, KH7, ESI-09, H89, anti-β-actin antibody, and anti-VSV-G antibody were purchased from Sigma-Aldrich. Ruxolitinib was from TargetMol. Fludarabine was obtained from Calbiochem. Polyinosinic-polycytidylic acid [poly(I:C)] was purchased from Invivogen. ADP-Glo™ Kinase Assay Kit was purchased from Promega. MRS 2211 and anti-GPR86 (P2Y$_{13}$) antibodies were purchased from Abcam. HJC0350 was purchased from Selleck. The anti-EPAC1 antibody was from Bioss. PrimeScript RT Master Mix and SYBR Premix Ex Taq were from Takara. IFN-α, IFN-β, and IFN-γ were purchased from Sino Biological Inc. The cAMP ELISA kit, mouse IFN-α/β receptor block/neutralize polyclonal goat IgG (AF1083), and normal goat IgG control were from R&D Systems. P2Y$_{13}$ plasmid was obtained from Biogot Technology, Co., Ltd.

Cell culture

The BMDMs were prepared as follows: bone marrow cells were collected from tibias and femurs by flushing with DMEM, and the cell suspension was filtered through a 40-μm cell strainer to remove any cell clumps. Bone marrow cells were then cultured in DMEM containing 10% FBS, 1% penicillin/streptomycin, and 20% L929 culture supernatants.

The PEMs were prepared as follows: mice were intraperitoneally injected with 3 ml of 4% sterile thioglycollate medium and, 3 days later, mice were sacrificed and the peritoneal cavities washed with 10 ml PBS. The cell suspension was filtered through a 70-μm cell strainer to remove any cell clumps. PEMs were then cultured in DMEM containing 10% FBS and 1% penicillin/streptomycin.

RAW264.7, HEK293T, and HeLa cells were obtained from the American Type Culture Collection and cultured in DMEM containing 10% FBS and 1% penicillin/streptomycin.

RNA extraction and quantitative real-time PCR

After stimulation, total RNA was extracted with RNAiso plus (TaKaRa) from the cells. cDNA was synthesized from extracted total RNA using the PrimeScript RT Master Mix Perfect Real Time Kit (TaKaRa) according to the manufacturer's protocol. Quantitative real-time PCR was performed using a SYBR-Green premix (Takara). The sequence-specific primers are listed in Supplementary Table S1.

ADP release assay

RAW264.7 cells, mouse BMDMs, and HEK293T cells were plated in 24-well plates (2×10^5 cells per well) overnight and then infected with viruses for various periods. ADP release into the cell culture supernatants was detected using ADP-Glo™ Kinase Assay Kit according to the manufacturer's protocol.

MTS assay

RAW264.7 cells were plated in 96-well plates (2×10^4 cells per well) overnight. The cells were treated with ADP for 6 h and then infected with VSV for 24 h. MTS (20 μl, Promega) was added to each well. After incubated for 1 h at 37°C, the absorption was measured at 490 nm. Cell viability of the untreated group was normalized to 100%.

Flow cytometry

HeLa and HEK293T cells were seeded into 24-well plates (1.5×10^5 cells per well) overnight. The cells were treated with ADP for 6 h and then infected with VSV-GFP or MLV-GFP for 24 h. Cells containing virus were determined after gating on GFP-positive cells.

Crystal violet staining assay

HEK293T cells were plated in 96-well plates (8×10^3 cells per well) overnight. Twelve hours after VSV (MOI = 0.01) or HSV-1 (MOI = 0.01) infection, cells were fixed with 4% paraformaldehyde in PBS for 20 min at room temperature. After incubation with crystal violet for 30 min, the cells were then washed with PBS five times before the photographs were taken.

Immunoblot

Cells were grown in 6-well plates. After stimulation, cells were lysed with radio immunoprecipitation assay (RIPA) buffer supplemented with protease and phosphatase inhibitors. Whole-cell lysates were separated by 10% SDS-PAGE, transferred to nitrocellulose membranes, and blocked with 5% BSA. Immunoblots were hybridized with the respective primary antibodies. Protein bands were visualized with the appropriate fluorescent secondary antibodies and the Odyssey laser digital imaging system (Gene Company).

Virus infection

Cells were infected with viruses for the indicated time and MOI. For mouse survival assay, 8-week-old P2Y$_{13}^{+/+}$ or P2Y$_{13}^{-/-}$ mice were intraperitoneally treated with ADP (50 mg/kg) or not treated for 6 h and then intraperitoneally injected with VSV (1×10^8 pfu/g). Executed these for 5 days and mouse survival was recorded for 10 days. For *in vivo* studies of viral replication, 6- to 8-week-old mice were intraperitoneally treated with ADP (50 mg/kg) or not treated for 6 h and then intraperitoneally injected with VSV (1×10^8 pfu/g) or HSV-1 (1×10^7 pfu/g) for the indicated time and viral RNA replicates in organs were detected by Q-PCR.

Viral plaque assay

Vero cells were plated in 12-well plates (2×10^5 cells per well) overnight. The supernatants from VSV-infected cells were serially diluted and infected Vero cells for 1 h. Then the supernatant was removed and the cells were covered with DMEM containing 1% low-melting point agarose. Plaques were counted after 20 h.

Immunofluorescence

For immunofluorescence assay, 6-week-old mice were anesthetized with ketamine/Rompun and treated with 5 mg/kg ADP through nasal dropping for 6 h before being intranasally infected with VSV (1×10^8 pfu/g). After 24 h of infection, mice were sacrificed, and the olfactories were fixed with 4% paraformaldehyde in PBS overnight. Slices (8-μm) from olfactories were permeabilized with 0.1% Triton X-100 and blocked with 5% BSA. Tissues were then incubated with anti-VSV-G antibody

overnight and Alexa-Fluor-488-conjugated secondary antibody for 2 h. Finally, the tissues were stained with DAPI and visualized with a fluorescence microscope.

ELISA

For cAMP detection, RAW264.7 cells or PEMs were plated in 6-well plates (1×10^6 or 2×10^6 cells per well, respectively) overnight. After stimulation, the cells were lysed with 200 μl cell lysis buffer and the amounts of cAMP were measured by ELISA (R&D Systems) according to the manufacturer's instructions.

Generation of EPAC1-knockout cell line

To generate an EPAC1-knockout cell line, a CRISPR/Cas9 system was used. The EPAC1-knockout target sequence used was 5′-AAATGCACTCCGGACCACG-3′. A Lenticrisprv2 plasmid containing the EPAC1-knockout target sequence was transduced into HeLa cells. Three days later, puromycin-resistant single clones were selected, and the EPAC1-knockout clones were identified by western blotting with the anti-EPAC1 antibody.

Statistical analysis

All data were analyzed using the GraphPad Prism software and shown as mean ± SD. The Student *t*-test (two-tailed) was used to analyze the significance of data and *P*-value <0.05 was considered statistically significant.

Supplementary material

Supplementary material is available at *Journal of Molecular Cell Biology* online.

Funding

This work was supported by the National Key R&D Program of China (2018YFA0507000 to B.D.), the National Natural Science Foundation of China (31570896 and 31770969 to B.D., 81672811 to M.Q.), Joint Research Institute for Science and Society (JoRISS) (14JORISS01 to B.D.), Science and Technology Commission of Shanghai Municipality (15JC1401500 to B.D.), and Innovation Program of Shanghai Municipal Education Commission (2017-01-07-00-05-E00011 to M.L.).

Conflict of interest: none declared.

References

Chen, W., Han, C., Xie, B., et al. (2013). Induction of Siglec-G by RNA viruses inhibits the innate immune response by promoting RIG-I degradation. Cell *152*, 467–478.

Chen, Y., Yao, Y., Sumi, Y., et al. (2010). Purinergic signaling: a fundamental mechanism in neutrophil activation. Sci. Signal. *3*, ra45.

Cho, J., Yusuf, R., Kook, S., et al. (2014). Purinergic $P2Y_{14}$ receptor modulates stress-induced hematopoietic stem/progenitor cell senescence. J. Clin. Invest. *124*, 3159–3171.

David, M., Petricoin, E., 3rd, and Larner, A.C. (1996). Activation of protein kinase A inhibits interferon induction of the Jak/Stat pathway in U266 cells. J. Biol. Chem. *271*, 4585–4588.

Di Virgilio, F., Dal Ben, D., Sarti, A.C., et al. (2017). The P2X7 receptor in infection and inflammation. Immunity *47*, 15–31.

Elliott, M.R., Chekeni, F.B., Trampont, P.C., et al. (2009). Nucleotides released by apoptotic cells act as a find-me signal to promote phagocytic clearance. Nature *461*, 282–286.

Eltzschig, H.K., Sitkovsky, M.V., and Robson, S.C. (2012). Purinergic signaling during inflammation. N. Engl. J. Med. *367*, 2322–2333.

Garcia, M.A., Gil, J., Ventoso, I., et al. (2006). Impact of protein kinase PKR in cell biology: from antiviral to antiproliferative action. Microbiol. Mol. Biol. Rev. *70*, 1032–1060.

Garcia-Sastre, A., and Biron, C.A. (2006). Type 1 interferons and the virus-host relationship: a lesson in detente. Science *312*, 879–882.

Gloerich, M., and Bos, J.L. (2010). Epac: defining a new mechanism for cAMP action. Annu. Rev. Pharmacol. Toxicol. *50*, 355–375.

Gong, B., Shelite, T., Mei, F.C., et al. (2013). Exchange protein directly activated by cAMP plays a critical role in bacterial invasion during fatal rickettsioses. Proc. Natl Acad. Sci. USA *110*, 19615–19620.

He, X., Ma, S., Tian, Y., et al. (2017). ERRα negatively regulates type I interferon induction by inhibiting TBK1-IRF3 interaction. PLoS Pathog. *13*, e1006347.

Idzko, M., Ferrari, D., and Eltzschig, H.K. (2014). Nucleotide signalling during inflammation. Nature *509*, 310–317.

Junger, W.G. (2011). Immune cell regulation by autocrine purinergic signalling. Nat. Rev. Immunol. *11*, 201–212.

Kawai, T., and Akira, S. (2010). The role of pattern-recognition receptors in innate immunity: update on Toll-like receptors. Nat. Immunol. *11*, 373–384.

Kobayashi, K., Yamanaka, H., Yanamoto, F., et al. (2012). Multiple P2Y subtypes in spinal microglia are involved in neuropathic pain after peripheral nerve injury. Glia *60*, 1529–1539.

Liu, S.Y., Aliyari, R., Chikere, K., et al. (2013). Interferon-inducible cholesterol-25-hydroxylase broadly inhibits viral entry by production of 25-hydroxycholesterol. Immunity *38*, 92–105.

Liu, X.Y., Chen, W., Wei, B., et al. (2011). IFN-induced TPR protein IFIT3 potentiates antiviral signaling by bridging MAVS and TBK1. J. Immunol. *187*, 2559–2568.

Liu, P.W., Yue, M.X., Zhou, R., et al. (2017). P2Y12 and P2Y13 receptors involved in ADPβs induced the release of IL-1β, IL-6 and TNF-α from cultured dorsal horn microglia. J. Pain Res. *10*, 1755–1767.

Lu, G., Reinert, J.T., Pitha-Rowe, I., et al. (2006). ISG15 enhances the innate antiviral response by inhibition of IRF-3 degradation. Cell. Mol. Biol. *52*, 29–41.

McDonough, K.A., and Rodriguez, A. (2011). The myriad roles of cyclic AMP in microbial pathogens: from signal to sword. Nat. Rev. Microbiol. *10*, 27–38.

Ooi, E.L., Chan, S.T., Cho, N.E., et al. (2014). Novel antiviral host factor, TNK1, regulates IFN signaling through serine phosphorylation of STAT1. Proc. Natl Acad. Sci. USA *111*, 1909–1914.

Platanias, L.C. (2005). Mechanisms of type-I- and type-II-interferon-mediated signalling. Nat. Rev. Immunol. *5*, 375–386.

Rafique, S., Idrees, M., Ilyas, M., et al. (2011). Positional effect of phosphorylation sites 266 and 267 in the cytoplasmic domain of the E2 protein of hepatitis C virus 3a genotype: interferon resistance analysis via sequence alignment. Virol. J. *8*, 204.

Ralevic, V., and Burnstock, G. (1998). Receptors for purines and pyrimidines. Pharmacol. Rev. *50*, 413–492.

Savi, P., Zachayus, J.L., Delesque-Touchard, N., et al. (2006). The active metabolite of Clopidogrel disrupts P2Y12 receptor oligomers and partitions them out of lipid rafts. Proc. Natl Acad. Sci. USA *103*, 11069–11074.

Shinozaki, Y., Shibata, K., Yoshida, K., et al. (2017). Transformation of astrocytes to a neuroprotective phenotype by microglia via P2Y1 receptor downregulation. Cell Rep. *19*, 1151–1164.

Shu, Q., Lennemann, N.J., Sarkar, S.N., et al. (2015). ADAP2 is an interferon stimulated gene that restricts RNA virus entry. PLoS Pathog. *11*, e1005150.

Tao, X., Mei, F., Agrawal, A., et al. (2014). Blocking of exchange proteins directly activated by cAMP leads to reduced replication of Middle East respiratory syndrome coronavirus. J. Virol. *88*, 3902–3910.

Vitiello, L., Gorini, S., Rosano, G., et al. (2012). Immunoregulation through extracellular nucleotides. Blood *120*, 511–518.

Wu, Y., Quan, Y., Liu, Y., et al. (2016). Hyperglycaemia inhibits REG3A expression to exacerbate TLR3-mediated skin inflammation in diabetes. Nat. Commun. *7*, 13393.

Yan, B.R., Zhou, L., Hu, M.M., et al. (2017). PKACs attenuate innate antiviral response by phosphorylating VISA and priming it for MARCH5-mediated degradation. PLoS Pathog. *13*, e1006648.

Zhan, Z., Cao, H., Xie, X., et al. (2015). Phosphatase PP4 negatively regulates type I IFN production and antiviral innate immunity by dephosphorylating and deactivating TBK1. J. Immunol. *195*, 3849–3857.

Zhang, D., Gao, Z.G., Zhang, K., et al. (2015). Two disparate ligand-binding sites in the human P2Y1 receptor. Nature *520*, 317–321.

Zhang, X., Qin, J., Zou, J., et al. (2018). Extracellular ADP facilitates monocyte recruitment in bacterial infection via ERK signaling. Cell. Mol. Immunol. *15*, 58–73.